14th International Congress on Artificial Materials for Novel Wave Phenomena – Metamaterials 2020
New York, USA, Sept. 28th – Oct. 3rd, 2020

Space-Time Non-Separability of Complex Electromagnetic Fields Generated by Metasurfaces

Yijie Shen[1], Apostolos Zdagkas[1], Nikitas Papasimakis[1], and Nikolay I. Zheludev[1,2]

[1] Optoelectronics Research Centre & Centre for Photonic Metamaterials, University of Southampton, Southampton SO17 1BJ, United Kingdom
[2] Centre for Disruptive Photonic Technologies, School of Physical and Mathematical Sciences and The Photonics Institute, Nanyang Technological University, Singapore 637378, Singapore

***Abstract* – We introduce a quantum mechanics inspired approach for the characterization of space-time non-separable waves, such as the Flying Doughnut pulse. We apply techniques analogous to quantum state tomography to quantify the type and degree of non-separability and provide quantitative predictions of the pulse propagation dynamics.**

I. INTRODUCTION

According to the traditional viewpoint, electromagnetic pulses are treated as space-time separable solutions of Maxwell's equations, that is their spatial and temporal dependence can be separated following the typical separation of variables for solving partial differential equations. However, a much broader family of electromagnetic waves, that exhibits space-time non-separability (STNS) and cannot be obtained or described in in this fashion, is known to exist [1-2]. Spurred by recent advances in topological optics and in our ability to control the spatiotemporal structure of light pulses, new types of waves with prescribed STNS are attracting growing attention, such as the "Flying Doughnut" (FD) pulses [3]. Indeed, FD pulses have emerged as a key component of toroidal electrodynamics particularly in the context of non-radiating anapole configurations and toroidal excitations in matter, as well as topological information transfer and probing light-matter interactions [4-6]. Here, we introduce a novel heuristic approach inspired by quantum state tomography for the characterization of space-time non-separable light pulses. We apply our methodology to complex pulses, such as the Flying Doughnut pulse and Laguerre-Gauss (LG) beams and quantify the type and strength of space-time coupling. We discuss the role of space-time coupling in the propagation dynamics.

II. RESULTS & DISCUSSION

We introduce our method by virtue of a characteristic example, the FD pulse. The electric field of a single-cycle transverse electric FD pulse is azimuthally polarized, whereas the magnetic field is oriented along the radial and longitudinal directions (see Fig. 1a). The pulse shape is controlled by two parameters, q_1 and q_2, corresponding to effective wavelength and Rayleigh range, respectively [3]. The pulse propagates similarly to a Gaussian pulse and experiences Gouy shift upon propagation, resulting in a change of temporal shape from 1½-cycle away from focus to single-cycle at focus. The STNS nature of the FD pulse manifests as isodiffraction, whereby all monochromatic components diffract at the same rate (see Fig. 1b), in contrast to common light pulses, such as a focused wide-band LG beam (see Fig. 1c).

Non-separability is, in fact, a quintessential property of quantum entanglement resulting in the development of an extensive toolbox for its quantitative description. Inspired by quantum mechanics methods, such as quantum state tomography [7], we introduce here an approach to quantify the strength of space-time (or equivalently space-spectrum) coupling in the isodiffracting FD pulse. Our approach is based on two sets of states: (1) Spectral states $|\lambda_i\rangle$ (i = 1, 2, …, n) - monochromatic states of light of prescribed wavelength λ_i; (2) Spatial states $|r_i\rangle$ - states of light at prescribed position r_i. The spectral and spatial states can be represented by the corresponding light fields, $E_{\lambda i}(r,z)$ and $E_{ri}(r,z)$, respectively. In the case of the FD pulse, the spatial and spectral states perfectly overlap and the pulse propagates with no distortion (Fig. 1b). In contrast, in the case of a conventional pulse, e.g. a wide-band Laguerre-Gauss (LG) pulse, which is also of toroidal topology but consists of a superposition of monochromatic LG beams, propagation leads to a mixing of the different monochromatic components and the pulse experiences substantial distortion in its spatio-spectral structure (Fig. 1c).

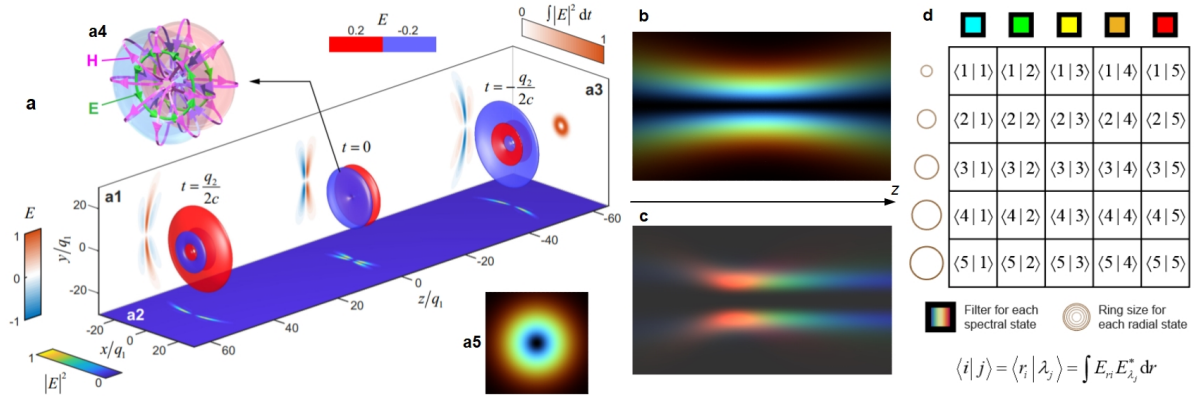

Fig. 1. (a) Spatiotemporal structure of the TE FD pulse (q_2=100q_1). The central plot shows spatial isosurfaces of the electric field $E(t,r,z)$ at different times, t = 0, $q_2/(2c)$,-$q_2/(2c)$ at amplitude levels ±0.2; a1, y-z map of the electric field E at x=0, at t=0, $q_2/(2c)$ and -$q_2/(2c)$; a2, x-z map of electric field intensity $|E|^2$ at x=0, at t=0, $q_2/(2c)$ and -$q_2/(2c)$; a3, x-y map of total electric field intensity $\int|E(t,r)|^2dt$ at the z=0 plane; a4, vector electromagnetic structure of the FD pulse, where green (magenta) represents electric (magnetic) field lines; a5, false-color image of the FD pulse in the x-y plane at its beam waist (z=0), where color corresponds to wavelength and brightness to intensity. (b-c) Comparison of propagation of an FD beam (b) to a wide-band LG beam (c) as represented by false color images in the x-z plane; for the isodiffracting FD beam, the spatiospectral structure is propagation invariant, in contrast to the wide-band LG beam. (d) Measuring STNS by state tomography. Spectral states correspond to the electric field profile of the monochromatic components of the pulse, while the radial states represent the field profile integrated over all wavelengths. Both spatial and spectral states are defined in relation to a specific x-y plane transverse to the propagation direction (z-axis). The tomography matrix is constructed by calculating the inner products between all spectral and radial states.

For the practical implementation of our method, the spectral $|\lambda_i\rangle$ and spatial $|r_i\rangle$ states at a specific transverse plane are approximated by the corresponding intensity profiles, $I_{\lambda i}$=$|E(\lambda_i)|$ring($r_{\lambda i}$,Δr) and I_{ri}=$\int|E(\lambda)|d\lambda$ring(r_i,Δr_i), where the ring function is ring(r_0,Δr_i)=1 if $r_0-\Delta r/2<r<r_0+\Delta r/2$ and is zero otherwise, and r_{λ_i} is the radial position at which the intensity of monochromatic component λ_i takes its peak value, and Δr_i=$|r_{\lambda i}-r_i|$ is the distance between the latter and the radial position of the spatial state. The electric field profile of a spectral state $|\lambda_i\rangle$, can be obtained by recording the intensity pattern of the pulse after propagation through a wavelength filter centered at λ_i. The spatial states are obtained in relation to the spectral states by calculating the theoretical intensity, $I^{(th)}(r_{\lambda i})$, at the position, $r_{\lambda i}$, and then finding the position, r_i, where the measured intensity is equal to the theoretical one $I^{(exp)}(r_i) = I^{(th)}(r_{\lambda i})$. The corresponding tomography matrix can be obtained by calculating the inner-product-like quantity $\langle\lambda_i|r_i\rangle$=$\int[I_{\lambda i}\, I_{ri}]^{1/2}dr$ at different propagation distances.

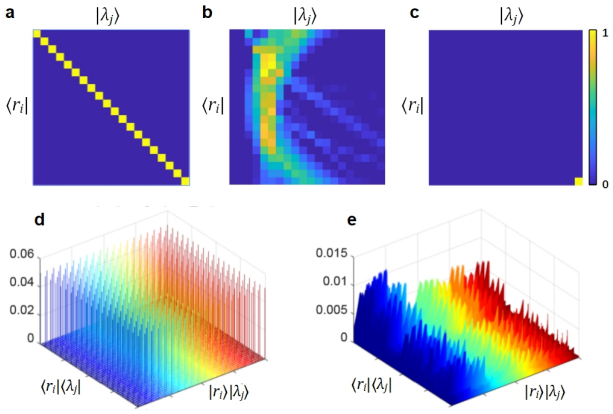

Fig. 2. (a-c), The results of state tomography for an FD pulse (a), a wide-band LG pulse (b), and monochromatic LG beam (c); In (a), the identity matrix indicates maximal space-spectrum entanglement, while in (b) the non-diagonal matrix reveals the breaking of space-spectrum entanglement. The monochromatic beam (c) exhibits a single non-zero matrix element highlighting its space-spectrum separable nature. (d-e) Reconstructed density matrices for the FD pulse (d) and the wide-band LG beam (e).

The tomography matrix for an FD pulse is always diagonal indicating maximum space-time entanglement (see Fig. 2a). In contrast, in the case of the wide-band LG pulse (see Fig. 2b), the tomography matrix exhibits dominant contributions from off-diagonal elements as a result of its non-isodiffracting nature. We also consider a monochromatic LG beam as an extreme case of complete absence of STNS, where only a single matrix element is non-vanishing (see Fig. 2c). Moreover, by reconstructing the corresponding density matrix, we can calculate the fidelity ($0<F<1$) which quantifies the similarity between the measured pulse and an FD pulse, where $F=1$ indicates a perfect FD pulse. For the wideband and monochromatic LG beams of Figs. 2b-c, fidelity approaches zero (0.01 and 0.04, respectively). Drawing further the analogy with quantum entanglement, we introduce concurrence (C) and entanglement of formation (E) as measures of STNS in isodiffracting pulses, where values close to unity indicate maximum STNS, whereas null values represent absence of STNS. Here the FD pulse exhibits strong STNS with unity concurrence and entanglement of formation, whereas in the case of the wideband LG beam STNS is substantially weaker with $C=0.89$ and $E=0.62$. Finally, in the case of a monochromatic beam both STNS measures vanish ($C=E=0$).

III. Conclusions

We propose a new approach inspired by quantum mechanics for the quantitative characterization of space-time (space-spectrum) non-separable pulses, such as the Flying Doughnut pulse. We introduce measures of space-spectrum entanglement for electromagnetic pulses analogous to the concurrence and entanglement of formation for quantum systems. We apply this methodology to two characteristic cases of complex non-separable pulses, the FD and a wideband LG beam with the former exhibiting substantially stronger STNS. The methodology introduced here provides quantitative means to guide the generation of such topological pulses. It can be readily applied to the characterization of space-time non-separability in various theoretical and experimental pulses and can be extended to different types of non-separability, such as the space-polarization non-separability observed in orbital angular momentum carrying waves.

References

[1] J. N. Brittingham, J. of Appl. Phys. 54, 1179 (1983).
[2] R. W. Ziolkowski, Phys. Rev. A 39, 2005 (1989).
[3] R. Hellwarth and P. Nouchi, Phys. Rev. E 54, 889 (1996).
[4] V. Savinov, N. Papasimakis, D. Tsai, and N. Zheludev, Commun. Phy. 2, 1 (2019).
[5] N. Papasimakis, V. Fedotov, V. Savinov, T. Raybould, and N. Zheludev, Nat. Mat. 15, 263 (2016).
[6] A. Zdagkas, N. Papasimakis, V. Savinov, M. R. Dennis, and N. I. Zheludev, Nanophotonics 8, 1379 (2019).
[7] E. Toninelli, B. Ndagano, A. Valles, B. Sephton, I. Nape, A. Ambrosio, F. Capasso, M. J. Padgett, and A. Forbes, Adv. Opt. Photonics 11, 67 (2019).